Montmorillonite-surfactant hybrid particles for modulating intestinal P-glycoprotein-mediated transport

Nielsen, Rasmus Blaaholm; Kahnt, Ariane; Dillen, Lieve; Wuyts, Koen; Snoeys, Jan; Nielsen, Ulla Gro; Holm, René; Nielsen, Carsten Uhd

Published in:
International Journal of Pharmaceutics

DOI:
10.1016/j.ijpharm.2019.118696

Publication date:
2019

Document Version
Peer reviewed version

Citation for published version (APA):
Nielsen, R. B., Kahnt, A., Dillen, L., Wuyts, K., Snoeys, J., Nielsen, U. G., Holm, R., & Nielsen, C. U. (2019). Montmorillonite-surfactant hybrid particles for modulating intestinal P-glycoprotein-mediated transport. *International Journal of Pharmaceutics*, *571*, [118696]. https://doi.org/10.1016/j.ijpharm.2019.118696

Montmorillonite-surfactant hybrid particles for modulating intestinal P-glycoprotein-mediated transport

Rasmus Blaaholm Nielsen[1], Ariane Kahnt[2], Lieve Dillen[2], Koen Wuyts[2], Jan Snoeys[2], Ulla Gro Nielsen[1], René Holm[3, 4], Carsten Uhd Nielsen[1*]

[1]Department of Physics, Chemistry and Pharmacy, University of Southern Denmark, Campusvej 55, DK-5230 Odense M, Denmark

[2]Drug Metabolism and Pharmacokinetics, Janssen R&D, Johnson & Johnson, Turnhoutseweg 30, BE-2340 Beerse, Belgium

[3]Drug Product Development, Janssen R&D, Johnson & Johnson, Turnhoutseweg 30, BE-2340 Beerse, Belgium

[4]Department of Science and Environment, Roskilde University, Universitetsvej 1, DK-4000 Roskilde, Denmark

*Corresponding author at: Department of Physics, Chemistry and Pharmacy, University of Southern Denmark, Campusvej 55, DK-5230 Odense M, Denmark, phone: +45 6550 9427, e-mail: cun@sdu.dk

Running title: MSH Particles increase digoxin exposure

Abstract

In the small intestine, P-glycoprotein (P-gp) may limit the permeability of its substrates, which lead to reduced oral absorption. To circumvent the effect of P-gp, a nanocomposite material termed *montmorillonite-surfactant hybrid particles* was developed. The particles consisted of montmorillonite, the P-gp-inhibiting, nonionic surfactant, polysorbate 20, and the P-gp substrate, digoxin. The present study aimed to investigate if montmorillonite-surfactant hybrid particles could modulate the absorption of digoxin *in vivo*. Montmorillonite-surfactant hybrid particles were prepared by lyophilising an aqueous suspension of the constituents. Scanning electron microscopy (SEM), thermogravimetric analysis (TGA), and powder X-ray diffraction (PXRD) revealed an altered surface morphology, decreased water content, and intercalation of polysorbate 20 between montmorillonite layers. The particles were administered orally to Sprague Dawley rats, and digoxin was quantified by liquid chromatography-tandem mass spectrometry. Control digoxin-containing montmorillonite decreased the exposure of digoxin. In contrast, montmorillonite-surfactant hybrid particles increased AUC and C_{max} by 31 and 91 %, respectively, compared to digoxin in solution. It was hypothesised that montmorillonite-surfactant hybrid particles increased digoxin exposure by forming mucosa-localised elevated concentrations of polysorbate 20 and digoxin, which enhanced the inhibitory effect of polysorbate 20 on P-gp.

Keywords: Intestinal absorption, montmorillonite, nanocomposites, digoxin, P-glycoprotein, polysorbate 20

Abbreviations: FWHM, the full width at half maximum; LBF, lipid-based formulation; MSH, montmorillonite-surfactant hybrid, P-gp, P-glycoprotein; SPE, solid phase extraction.

List of compounds studied: Polysorbate 20, montmorillonite, digoxin.

1 Introduction

Pharmacokinetic properties of drug substances have gained increased focus in early drug development, as an estimated 10-20 % of drug candidates fail in preclinical development or in clinical trials, because of undesirable pharmacokinetic properties (Cook et al., 2014; Di and Kerns, 2016; Kola and Landis, 2004). These undesirable pharmacokinetic properties are often caused by P-glycoprotein (P-gp) (Di and Kerns, 2016), which is a widely expressed efflux transporter (Thiebaut et al., 1987). In the apical membrane of the intestinal epithelium, P-gp mediates cellular efflux of numerous drug substances, which leads to decreased absorption and bioavailability of the drug substance in question (Leslie et al., 2005; Lin and Yamazaki, 2003).

Numerous nonionic surfactants have been shown to inhibit P-gp in cell- and animal models, albeit in relatively high concentrations (Al-Ali et al., 2019; Cornaire et al., 2004; Lo, 2003; Zhang et al., 2003). Polysorbate 20 is among the most potent surfactant-based P-gp inhibitors investigated (Al-Ali et al., 2018a; Al-Ali et al., 2018b; Al-Saraf et al., 2016; Gurjar et al., 2018; Lo, 2003). Co-administration of 0.55 g kg^{-1} polysorbate 20 significantly increased the oral bioavailability of the P-gp substrate, digoxin, in rats from 59 to 84 %, and increased C_{max} by 79 % (Nielsen et al., 2016). Corresponding administration of digoxin to *mdr1a* knockout rats produced an increased bioavailability, and there was no effect of co-administration of polysorbate 20 (Nielsen et al., 2016). This suggested that solubilising effects and/or increased passive permeability were not the cause of the increased absorption in wild type rats. However, a polysorbate 20 dose of 0.55 g kg^{-1} corresponds to a dose of approximately 6 g in humans, when a simple proportional weight scaling is applied (Nair and Jacob, 2016), i.e., more than thrice that of the WHO-recommended maximal daily dose of 25 mg kg^{-1} (Sheskey et al., 2017). Thus, there is a need to potentiate the effects of polysorbate 20 on P-gp to develop an applicable polysorbate 20-based formulation for intestinal P-gp inhibition.

In vitro, only 200 µM (246 µg mL^{-1}) polysorbate 20 was required to completely inhibit P-gp-mediated digoxin efflux in Caco-2 cells (Nielsen et al., 2016). Meanwhile, 10 % v/v (110 mg mL^{-1}) polysorbate 20 in the dosing solution was necessary to produce the highest observed inhibition of intestinal P-gp activity, *in vivo* (Nielsen et al., 2016). This 450-fold difference could be related to the fact that the *in vitro* transport system is stationary, while the intestinal lumen is a dynamic system with intestinal dilution, intestinal transit, and a redundancy in the area able to mediate absorption. Therefore, a formulation approach may be applied, in which polysorbate 20 and digoxin are released in the vicinity of the epithelial cells to modify the absorption process. We hypothesise that the clay nanomaterial, montmorillonite, can be applied as a drug substance- and excipient carrier in this context.

Montmorillonite has previously been investigated as a drug carrier (Aguzzi et al., 2007; Ruiz-Hitzky et al., 2010). Montmorillonite, like other clays, has a distinct layered structure and surface chemistry, and montmorillonite elicits a strong ability to retain cations (Hensen and Smit, 2002). Countless complex possibilities exist when montmorillonite is combined with for example polymers, surfactants, and dyes to form nanocomposites. Many potential applications have been investigated from wound dressings to food packaging and waste water treatment (Kokabi et al., 2007; Rhim et al., 2013; Wang and Wang, 2007). However, the application of montmorillonite-based nanocomposites has received limited attention in the pharmaceutical field. The most common approach has been to intercalate cationic drug substances between montmorillonite layers to obtain either a modulated drug release or a solubilising effect on the drug substance in question (Aguzzi et al., 2007). Neutral drug substances have also been shown to adsorb to montmorillonite surfaces via ion-dipole interactions (Su and Carstensen, 1972), and montmorillonite has been recognised as a possible solid carrier for lipid-based formulations (LBF) (Dening et al., 2017; Dening et al., 2018; Feeney et al., 2016). Calabrese and co-workers have successfully incorporated polysorbate 20 in montmorillonite to obtain delayed release of cinnamic acid (Calabrese et al., 2016; Calabrese et al., 2017), and they showed that

polysorbate 20 facilitated the release of cinnamic acid from montmorillonite. Their studies also confirm the strong interactions between montmorillonite and polymers or surfactants that contain oxyethylene groups (-CH_2-CH_2-O-), like polysorbate 20 (Aranda and Ruiz-Hitzky, 1992). Additionally, it has been shown that montmorillonite has mucoadhesive properties. For example, it was shown that montmorillonite intercalated with tetracycline displayed mucoadhesive forces to porcine mucus corresponding to 43 % of chitosan, which is a known highly mucoadhesive polysaccharide (Iannuccelli et al., 2015). As a result, studies have focused on montmorillonite and composites hereof to obtain mucoadhesive drug delivery systems for gastroretention or local oral administration (Aguzzi et al., 2007; Calabrese et al., 2013; Iannuccelli et al., 2015; Onnainty et al., 2016).

Montmorillonite or other clay-based nanomaterials have not been investigated in pharmaceutical science to obtain modulation of intestinal drug transporters, to our knowledge. Based on literature findings that montmorillonite has mucoadhesive properties and displays modified drug substance release in combination with polysorbate 20, we hypothesise that montmorillonite-surfactant hybrid (MSH) particles intercalated with polysorbate 20 and digoxin may lead to increased exposure of digoxin, compared to corresponding doses of polysorbate 20 and digoxin in simple solutions. The present study aimed to prepare and characterise MSH particles and to assess the pharmacokinetics of digoxin in rats after administration as MSH particles, compared to administration as simple solutions containing polysorbate 20.

2 Materials and methods

2.1 Materials

Digoxin, triple deuterated (D_3)-digoxin, polysorbate 20, bovine serum albumin (albumin fraction V) > 97 %, montmorillonite as ‘nanoclay, hydrophilic bentonite’, and all other chemicals in analytical grade quality or higher were from Merck KGaA (Germany). Ultrapure water was obtained from an

in-house Milli-Q purification system (Millipore, MA, USA). Blank rat plasma was from Bioreclamation IVT (NY, USA).

2.2 Preparation of montmorillonite-surfactant hybrid particles

MSH particles were prepared with a fixed 1:1 w/w ratio of montmorillonite and polysorbate 20 along with an amount of digoxin that allowed a constant digoxin dose and variable doses of montmorillonite and polysorbate 20 (Table 1). Furthermore, two control formulations were prepared. One contained montmorillonite and digoxin, designated *digoxin-containing montmorillonite*, and one contained only montmorillonite, designated *lyophilised montmorillonite*.

Suspensions of montmorillonite, polysorbate 20, and digoxin were obtained by suspending montmorillonite in 11.0 mL ultrapure water (Milli-Q) in a beaker fitted with a magnet and stirred for 4 h. The pH was 9.5 after hydration of the montmorillonite suspension, and the pH was subsequently adjusted to 7.0 ± 0.1 with HCl. In parallel, polysorbate 20 was added to a screwcap vial together with 1000 µL of a 1.00 mg mL^{-1} digoxin stock solution in 96 % v/v ethanol. The mixture was ultrasonicated for 30 min to ensure solubilisation of digoxin using an Elmasonic P30H ultrasonic bath (Elma Schmidbauer, Germany). 12.0 mL of ultrapure water was then added, and the polysorbate 20-digoxin mixture was ultrasonicated for 60 min to aid micelle formation. Then, the polysorbate 20-digoxin solution was added to the montmorillonite suspension dropwise (5 min), and the resulting suspension was stirred for 24 h with the pH maintained at 7.5 ± 0.5 by manual addition of microvolumes of 1 M HCl. The suspension was divided into ten separate 10 mL lyophilisation vials and stored at -20 ^{o}C overnight. The frozen suspensions were lyophilised in a Beta 2-8 LSCBasic table top freeze dryer (Martin Christ, Germany). Main drying lasted for 40 h, applying a system pressure of 0.200 mbar, a shelf temperature of -25 ^{o}C, and a condenser temperature of approximately -85 ^{o}C. The final drying lasted for 4 h, applying a system pressure of 0.011 mbar, a shelf temperature of 25 ^{o}C, and a condenser temperature of approximately -85^{o}C. Following lyophilisation, the chamber was filled with dry N_2

gas, and the vials were quickly equipped with rubber stoppers. The total MSH particle content in each vial was assessed by weighing the vial before filling and after lyophilisation. The products appeared either as cakes or powders depending on the concentration of montmorillonite in the final suspensions with increasing montmorillonite amounts resulting in a stable cake.

2.3 Characterisation of MSH particles

The MSH particles were characterised by scanning electron microscopy (SEM), thermogravimetric analysis (TGA), and powder X-ray diffraction (PXRD).

2.3.1 Scanning electron microscopy

SEM was carried out with a Phenom ProX scanning electron microscope (Thermo Fisher Scientific, MA, USA). A small amount of powder was mounted on 12 mm stubs with carbon tabs (Agar Scientific, UK) and coated with gold by a Q150S rotary-pumped sputter coater-carbon coater (Quorum, UK). Imaging was carried out at an accelerating voltage of 5 kV at magnifications ×175-2900 and 10 kV at magnifications ×4300-29000.

2.3.2 Thermogravimetric analysis

TGA was carried out on a Q500 thermogravimetric analyser (TA Instruments, TX, USA). Samples of 2-4 mg was equilibrated at 30 ^{o}C for 2 min before the temperature was increased to 700 ^{o}C at a rate of 10 ^{o}C min^{-1}.

2.3.3 Powder X-ray diffraction

PXRD was carried out with a PANalytical X'pert PRO multipurpose diffractometer (Malvern Panalytical, UK). Scanning was performed with a Cu Kα, λ = 1.5406 Å radiation source in the 2θ range from 3 to 50 ^{o} with a scan speed of 0.254 ^{o} s^{-1} and a step size of 0.0167 ^{o}. The voltage and current were set to 45 kV and 40 mA, respectively. Samples were prepared on 16 mm zero background plates.

Miller indices were applied to describe the lattice planes in a sample that caused the observed reflections in powder X-ray diffractograms. A lattice plane can be described by three integers (*hkl*), and the main interest of the present study was the (001) reflection, which is the reflection corresponding to the distance between two individual montmorillonite layers. Reflections caused by lattice planes within the individual montmorillonite layers, which were not related to interlayer distance, can be described as *(hk0) reflections*. The interlayer spacing of montmorillonite was calculated from the diffraction angles at maximum intensity of (001) reflections using Bragg's law:

$$n\,\lambda = 2d\,\sin(\theta) \qquad \text{(I)}$$

where n is the number of wavelengths, λ is the wavelength of the X-ray source, d is the interlayer spacing, and θ is the diffraction angle. Reflections were assigned by a comparison with literature (Viani et al., 2002). The full width at half maximum (FWHM) was estimated by manual readouts.

2.4 In vivo *study*

The study was carried out in accordance with European and Belgian law controlling the experiments on animals. 60 male Sprague Dawley rats (10 groups, n=6) were supplied from Charles River (MA, USA) and acclimatised 11-12 days before conductance of the study. At the beginning of the study, the animals weighed 245-300 g (approximately 9 weeks of age) and were fasted for about 16 h prior to the experiment.

Animals were dosed by oral gavage with 5 mL kg^{-1} solutions or suspensions containing 0.02 mg kg^{-1} digoxin in 40 % v/v ethanol in water. Dosing overview of the individual groups is shown in Table 2. The amount of ethanol administered did not affect the rats' clinical behaviour.

Blood samples were taken 15, 30, 45, 60, 120, 180, 240, and 360 min after administration. Micro sampling was performed by placing the rats in a restrainer and puncturing the tail vein with a 25G needle. 64 µL of blood was then collected in a glass capillary (Vitrex Medical, Denmark) and closed

179 in one end with a sigillum wax plate (Vitrex Medical, Denmark). Capillaries containing blood
180 samples were placed in centrifuge tubes and kept on ice until centrifugation (1900 G, 4 ^{o}C, 10 min).
181 After centrifugation, the clear part of the capillary, containing plasma, was cut off, and the plasma
182 was transferred to two 10 µL end-to-end pipettes (Vitrex Medical, Denmark) and placed in two
183 individually labelled 1 mL Fluid X tubes (Brooks Life Sciences, MA, USA) with lids and stored in a
184 96-well format. Samples were kept at -20 ^{o}C until analysis. The rats were euthanised after the last
185 blood sample.

186 *2.4.1 Bioanalysis*

187 Calibration standards of digoxin were prepared in rat plasma to obtain concentrations of
188 2-100 ng mL^{-1}. Quality control samples of 8, 50, and 100 ng mL^{-1} solutions were prepared by spiking
189 rat plasma with appropriate amounts of digoxin stock solution. Calibration standards and quality
190 control samples were stored in 10 µL end-to-end pipettes placed in Fluid X tubes and kept in a freezer
191 (-20 ^{o}C) until sample preparation and were treated like the plasma samples as described below.

192 To wash out sample plasma from the end-to-end pipettes, 100 µL 2 % w/v bovine serum albumin in
193 phosphate buffer (pH 7.5) was added to the sample tubes, and the samples were shaken horizontally
194 (10 min, 500 min^{-1}) and subsequently centrifuged (5 min, 20 ^{o}C, 2300 × g). A 55 µL aliquot of the
195 sample was then transferred to a new Fluid X tube, and 55 µL internal standard (25 ng mL^{-1} D_3-
196 digoxin in methanol) was added. The pH of the resulting mixture was adjusted to 9 by addition of 25
197 µL of a 2 M ammonium acetate solution followed by dilution with 175 µL Milli-Q purified water.
198 The samples were shaken by vortex mixing after each addition.

199 Oasis® HLB 96 well solid phase extraction (SPE) plates, 30 µm particle size, 30 mg sorbent per well
200 (Waters, MA, USA) were conditioned with 1 mL methanol, 1 mL Milli-Q purified water, and 3 × 0.5
201 mL 0.1 M ammonium acetate (pH 9). Positive pressure (~ 3 psi) was applied after each addition, until

202 the resin was dry. Subsequently, the entire sample volume (310 µL) was transferred to the conditioned
203 SPE well plates and positive pressure (~ 1.5 psi) was applied to load the samples slowly. The SPE
204 wells were then washed with 3 × 0.5 mL 0.1 M ammonium acetate (pH 9). A positive pressure
205 (~ 3 psi) was applied after each addition, until the resin was dry. The samples were then eluted from
206 the SPE resin with 2 × 0.5 mL and 1 × 0.2 mL ethanol into a new 96-well plate. The eluent was then
207 dried under a 40 L min^{-1} flow of dry N_2 at room temperature (Porvair Minivap, Porvair Sciences, UK)
208 and reconstituted in 300 µL 1:1 methanol:water mixture followed by vortex mixing. After a
209 centrifugation step (10 min, 6000 × g) the samples were transferred to a round 96-well plate for
210 chromatographic analysis.

211 Liquid chromatography-tandem mass spectrometry (LC-MS/MS) analysis was carried out on a 6500
212 Sciex triple quad instrument (ABSciex, Canada), which was coupled to a UHPLC-system (Shimadzu,
213 Japan). The chromatographic separation was carried out using a reversed phase UPLC column
214 (Acquity BEH C18, 1.7 µm, 50×2.1 mm, Waters, MA, USA). The mobile phases consisted of 0.01 M
215 ammonium carbonate (solvent A) and methanol (solvent B), and a gradient elution at 45 °C was
216 performed (starting at 50 % solvent A, 50 % solvent B to 75 % solvent B in 2.3 min, followed by
217 isocratic hold at 95 % B for 1.19 min and re-equilibration to 50 % B in 0.99 min). Total run time was
218 4.5 min and a flow rate of 0.3 mL min^{-1} was applied.

219 The LC-MS/MS was operated in positive ion mode using the TurboIonSpray™-interface
220 (electrospray ionisation), and was optimised for the quantification of digoxin, applying multiple
221 reaction monitoring (*m/z* 798.6 → *m/z* 651).

222 The calibration curve ranged from 2-100 ng mL^{-1} and linear regression with a weighing factor of $1/x^2$
223 was used to produce the best fit for the concentration-detector response relationship. The lower limit
224 of quantification was 2 ng mL^{-1}. The accuracy of all batches, as measured by independent quality

control samples, were between 80-120 % of the nominal value over the entire range for the plasma samples.

2.4.2 Data analysis

The AUC of digoxin in the pharmacokinetic profile in the range 0-6 h was calculated by the trapezoidal method. First order elimination was assumed, and the elimination rate constant (k_e) of digoxin was estimated by performing linear regression of Ln to the plasma concentrations as a function of time using data points at 2, 3, 4, and 6 h. The slope of the resulting regression was $-k_e$. R^2 values were generally above 0.90. Plasma profiles were also fitted to zero order elimination with a simple linear regression for the time points stated above. All formulations, except digoxin-containing montmorillonite, displayed a higher R^2 of the fit with first order elimination. It was assumed that the formulations did not affect elimination, and that the difference observed for digoxin-containing montmorillonite was caused by prolongation of absorption into the elimination phase, rather than altered elimination. For this reason, plasma profiles for the treatment with digoxin-containing montmorillonite was still analysed as first order elimination.

The $t_{½}$ of digoxin was calculated:

$$t_{½} = \frac{\ln(2)}{k_e} \quad \text{(II)}$$

Each analysis of $AUC_{0\text{-}6h}$ and elimination was performed for each individual data set, before statistical analysis.

2.4.3 Statistical analysis

Statistical analysis was performed in GraphPad Prism 8.1.2. The pharmacokinetic parameters, $AUC_{0\text{-}6h}$, C_{max}, the plasma concentration at the first sampling point ($C_{15\ min}$), and $t_{½}$ of each group of animals were compared by one-way ANOVA, followed by a Dunnett's test in the following order: Co-administration of the three doses of polysorbate 20 was compared to digoxin administered alone,

and administration of MSH particles A-E was compared to both digoxin administered alone and to digoxin-containing montmorillonite in two separate analyses. A student's t test was applied to compare the pharmacokinetic parameters after administration of digoxin-containing montmorillonite and digoxin only. All P-values below 0.05 were considered statistically significant.

3 Results

3.1 Characterisation of MSH particles

The untreated montmorillonite was light-brown or beige, as was the lyophilised- and digoxin-containing montmorillonite formulations without polysorbate 20. In contrast, polysorbate 20-containing MSH particle formulations were more pale and had an off-white colour.

3.1.1 Scanning electron microscopy

The shape and surface morphology of the montmorillonite particles was investigated by SEM. Untreated montmorillonite (Fig. 1A) contained pores of irregular shape with the observed perimeter diameters in the range 0.8-2.5 µm. The surface morphology of digoxin-containing (Fig. 1B) and lyophilised montmorillonite (Fig. S2B) appeared similar on the SEM images. Comparison of the SEM images of untreated montmorillonite with lyophilised montmorillonite and digoxin-containing montmorillonite, showed that lyophilisation resulted in a more porous structure with pore diameters of 0.5-3 µm, which was also observed when polysorbate 20 was intercalated (Fig. 1C and D). Additionally, when polysorbate 20 was intercalated, the pores and the appearance of the particle surface for MSH particles changed to smoother and more circle- or ellipse-shaped pores, as compared to digoxin-containing and lyophilised montmorillonite.

The particle shape changed from spheres to irregular particles with sharp edges upon lyophilisation (Fig. S1). The observed perimeter diameter of the untreated montmorillonite particles was in the range of 4-50 µm. The irregular MSH particles and digoxin-containing montmorillonite was in the range of 2-200 µm, while lyophilised montmorillonite was in the range of 2-500 µm (Fig. S2A).

3.1.2 Thermogravimetric analysis

The composition and stability of the starting compounds and the prepared formulations were assessed by TGA (Fig. 2). The characteristic temperature intervals and corresponding thermogravimetric mass loss are given in Table S1. Untreated montmorillonite contained 11 % physically adsorbed water and 4 % interlayer water. Dehydroxylation of the untreated montmorillonite accounted for a 3 % mass loss, resulting in a mass of 83 % left in the pan after heating to 700 ^{o}C (residual mass). Polysorbate 20 contained 2 % water and 96 % mass was lost during degradation, which left a residual mass of 1 %.

Lyophilised and digoxin-containing montmorillonite contained less physically adsorbed water than untreated montmorillonite with 5 and 7 %, respectively, and 4 % interlayer water. Furthermore, lyophilised and untreated montmorillonite displayed an 87 % and 86 % residual mass, respectively (Table S1). These residuals correspond to untreated montmorillonite, when corrected for water content.

MSH particles displayed an even lower content of both physically adsorbed water at 1 % and interlayer water at 1 %. Degradation of polysorbate 20 led to a 53 % mass loss, and montmorillonite dehydroxylation accounted for 1 % mass loss, which resulted in a 45 % residual, corresponding to montmorillonite content. Additionally, comparison of polysorbate 20 and MSH particles showed that polysorbate 20 decomposed at a lower temperature, when it was incorporated into MSH particles as the polysorbate 20 degradation was shifted approximately 35 ^{o}C down.

3.1.3 Powder X-ray diffraction

The interlayer spacing of montmorillonite in the MSH particles was investigated by PXRD, as shown in Fig. 3. The interlayer spacing, which was determined from the (001) reflection was 14.9 Å in untreated montmorillonite and increased to 18.0 Å in MSH particles. The (001) reflection for untreated montmorillonite displayed a FWHM of 1.66 °, while the (001) reflection of MSH particles

was narrower with a FWHM of 1.00 °. Additionally, the (002), (003), (005), and (006) reflections were present in the MSH particle diffractogram, but not in the untreated montmorillonite diffractogram. For both digoxin-containing montmorillonite and lyophilised montmorillonite, none of the (00*l*) reflections were observed (Fig. 3).

At larger diffraction angles, all formulations showed reflections at approximately 20, 35, and 40 °. They can all be assigned to (*hk*0) reflections or combinations including these, which were all independent of the orientation of the individual montmorillonite layers. Reflections at 29 ° were only present for untreated montmorillonite, digoxin-containing montmorillonite, and lyophilised montmorillonite.

3.2 *In vivo* study

The pharmacokinetics of digoxin was investigated in male Sprague Dawley rats, when polysorbate 20 was co-administered in simple solutions and in MSH particles. The pharmacokinetic profiles are shown in Fig. 4, while obtained pharmacokinetic parameters are summarised in Table 3. The effects of the applied formulations were most notable on C_{max} and $C_{15\ min}$. Overall, the plasma concentration of digoxin reached a maximum within the first 45 min (Table 3). Elimination generally followed first order kinetics and there was no apparent correlation between formulation type and $t_{½}$ (Table 3).

Formulations that contained polysorbate 20 in simple solutions did not alter $AUC_{0\text{-}6h}$. However, they tended to decrease t_{max} and increase C_{max} and $C_{15\ min}$ of digoxin (Fig. 4A). $C_{15\ min}$ was increased in a statistically significant manner for co-administration of 55 and 274 mg kg^{-1} polysorbate 20 (Table 3).

When digoxin was administered as digoxin-containing montmorillonite, a great alteration of the pharmacokinetic profile was observed (Fig 4B). Administration of digoxin-containing montmorillonite resulted in significantly lowered $AUC_{0\text{-}6h}$, C_{max} and $C_{15\ min}$, compared to digoxin only (Table 3), and C_{max}/t_{max} could not clearly be defined (Fig 4B).

In contrast, when digoxin was administered as MSH particles, containing montmorillonite *and* polysorbate 20, $AUC_{0\text{-}6h}$, C_{max}, and $C_{15\ min}$ all increased 2-4-fold, compared to digoxin-containing montmorillonite (Table 3). For doses of 137-548 mg kg^{-1} montmorillonite and polysorbate 20, these increases were statistically significant. In concordance, the incorporation of polysorbate 20 also led to decreased t_{max} (Table 3). Compared to digoxin administered alone, MSH particles increased $AUC_{0\text{-}6h}$, C_{max} and $C_{15\ min}$, and the increase in C_{max} and $C_{15\ min}$ for the 548 mg kg^{-1} MSH formulation was statistically significant (Table 3).

In some cases, MSH particles also tended to increase both $AUC_{0\text{-}6h}$ and C_{max} of digoxin, compared to co-administration of polysorbate 20 in simple solutions in the corresponding doses. For example, co-administration of 548 mg kg^{-1} polysorbate 20 as MSH particles increased $AUC_{0\text{-}6h}$ and C_{max} of digoxin 31 % and 32 %, compared to co-administration of 548 mg kg^{-1} polysorbate 20 in a simple solution (Fig. 4D).

4 Discussion

4.1 Polysorbate 20 is intercalated in MSH particles

The obtained MSH particles were solid, even though they consisted of 52 % polysorbate 20, which is liquid at room temperature. This phase transition may occur, because polysorbate 20 was adsorbed to the montmorillonite surfaces. This was supported by the lighter colour of the MSH particles, which indicated that polysorbate 20 coated the montmorillonite surface, as also reflected by the particle morphology according to SEM. Lyophilised montmorillonite, digoxin-containing montmorillonite, and MSH particles were subjected to the same lyophilisation cycle, but the total water content was considerably lower in MSH particles. The lower interlayer water content suggested that the intercalation of polysorbate 20 led to extrusion of water from the interlayer spaces. The destabilisation of polysorbate 20, when incorporated in MSH particles, as indicated by TGA, was also observed by

340 Calabrese and co-workers (Calabrese et al., 2016), and similar trends have been presented with similar
341 nanocomposites (Liu et al., 2003).

342 The structure of individual montmorillonite layers was conserved in all the samples, as evident by the
343 combined (hk0) reflections obtained with PXRD. The (001) reflection shifted to a lower diffraction
344 angle for MSH particles as compared to untreated montmorillonite, which implied an increased
345 interlayer distance from 14.9 to 18.0 Å. This 3.1 Å increase agrees well with previous studies
346 (Calabrese et al., 2016; Calabrese et al., 2017). Under the assumption that the thickness of an
347 individual montmorillonite layer is 10 Å (Ploehn and Liu, 2006), the resulting distance between
348 individual montmorillonite layers was 8 Å, corresponding to 5-6 C-C alkane bonds (Skinner, 1945).
349 This distance indicated a relatively flat conformation of polysorbate 20, and effectively excluded the
350 possibility of micelle-like bilayer conformations or similar.

351 The (001) reflection was absent in digoxin-containing and lyophilised montmorillonite, which
352 implied exfoliation of montmorillonite layers as illustrated in Fig. 5. Furthermore, the appearance of
353 (002), (003), (005), and (006) and a narrower (001) reflection in the MSH particle diffractogram
354 suggested increased stacking order. Hence, lyophilisation of montmorillonite suspensions seems to
355 lead to exfoliation of individual layers. In contrast, when polysorbate 20 was introduced in the
356 preparation of MSH particles, which were subjected to the same lyophilisation cycle, montmorillonite
357 layers were not exfoliated. Instead, polysorbate 20 assisted in the stacking of montmorillonite layers
358 and increased the stacking order of montmorillonite layers.

359 The presence of the reflection at 29 ^{o} for untreated montmorillonite and digoxin-treated
360 montmorillonite and the absence of the same reflection for MSH particles has not conclusively been
361 understood. The reflection could simply have been overshadowed in the diffractogram of MSH
362 particles.

Characterisation of MSH particles by SEM, PXRD, and TGA have proven a strong interaction between polysorbate 20 and montmorillonite. Many different interactions between clays and organic compounds have previously been described (Ruiz-Hitzky et al., 2010). Some of those are also suggested here: i) ion-dipole interactions between oxyethylene (-CH_2-CH_2-O-) units of polysorbate 20 and the negative surface charge of montmorillonite; ii) hydrogen bonding between end hydroxyl groups of polysorbate 20 and the siloxane surface of montmorillonite.

4.2 Polysorbate 20-containing solutions modulated digoxin pharmacokinetics

The experimental design did not allow for thorough estimation of digoxin absorption rate constant from the intestine, and for this reason, the first sampling point at 15 min was taken as a rough estimate of absorption rate. Polysorbate 20 in the simple solution tended to increase C_{max} and $C_{15\ min}$ and decreased t_{max}, which was also shown by Nielsen and co-workers in a previous study (Nielsen et al., 2016). However, in contrast to this previous study, no change was observed in $AUC_{0\text{-}6h}$ in the present study. Overall, AUC-values were generally lower in the present study compared to the study by Nielsen and co-workers. This may partly be caused by the inclusion of the $AUC_{6\text{-}\infty}$ part by Nielsen and co-workers, which was not included in the present study. The less pronounced effect of polysorbate 20 on digoxin pharmacokinetics may also partly be attributed to differences in quantification methods and variation between animals and raw materials. Variation of the composition between brands and lots of polysorbate 20 is well-documented (Hewitt et al., 2011), which may influence the function of polysorbate 20 as a P-gp inhibitor. Furthermore, previous studies on inhibition of intestinal transporters and carriers have also shown a clear modulation of the pharmacokinetic profile and effects on C_{max} and t_{max}, but with no effects on AUC (Broberg et al., 2012; Nohr et al., 2014). When preceding evidence is considered, the present study still indicates that polysorbate 20 modulated the pharmacokinetics of digoxin, despite limited statistical strength. The

modulation of digoxin pharmacokinetics was ascribed to the inhibition of intestinal P-gp, leading to lowered efflux, and increased intestinal absorption of digoxin.

4.3 Montmorillonite-surfactant hybrid particles increased digoxin exposure

When digoxin-containing montmorillonite was administered, the $AUC_{0\text{-}6h}$, C_{max}, and $C_{15\ min}$ decreased compared to digoxin only, likely because of retention of digoxin by montmorillonite in the formulation, which led to less digoxin available for absorption. This phenomenon has also been observed by Dening and co-workers (Dening et al., 2018) when the lipophilic and cationic drug substance, blonanserin, was intercalated into montmorillonite. Dening and co-workers investigated blonanserin release from montmorillonite in a USP dissolution setup, where only 13 % was released after 12 h. Accordingly, bioavailability in Sprague Dawley rats for montmorillonite-intercalated blonanserin was reduced by 35 %, compared to the pure drug suspension (Dening et al., 2018). The retention of digoxin in the present study showed that montmorillonite can also effectively adsorb uncharged drug substances. Therefore, montmorillonite alone appeared to be unsuitable for increasing oral digoxin absorption. Nevertheless, the lowering of digoxin exposure by digoxin-containing montmorillonite was contrasted by the tendency of the MSH particles to increase the exposure of digoxin. We therefore suggest that polysorbate 20 facilitated digoxin release from the MSH particles and also inhibited P-gp activity, leading to an increased digoxin exposure. At present, it was not possible to unequivocally distinguish these two effects from each other. Additionally, we suggest that local co-release of digoxin and polysorbate 20 may have caused the observed increased exposure by elevation of both polysorbate 20- and digoxin mucosal concentrations, compared to polysorbate 20 and digoxin in simple solutions. However, neither the physicochemical characterisation nor the *in vivo* performance of MSH particles have been able to confirm the underlying mechanism, and further studies of the MSH particle-mucosa interaction are needed.

When the effects of MSH particles and digoxin-containing montmorillonite are compared, montmorillonite exhibited a dual function with respect to digoxin retention and enhancement of P-gp inhibition. This was observed as a decreased digoxin exposure for digoxin-containing montmorillonite, relative to control, but also as an enhancement of digoxin exposure, when montmorillonite was intercalated with polysorbate 20 in MSH particles. The observed effects of digoxin-containing montmorillonite and MSH particles *in vivo* and the proposed mechanisms have been illustrated in Fig. 5.

Clays and other solid carriers have also been applied to solidify LBFs, and some examples exists, where the solidified LBF outperforms the liquid LBF *in vivo* (Dening et al., 2018; Tan et al., 2013) – similarly to what have been observed in the present study. For example, a solidified silica-lipid hybrid formulation of blonanserin tended to increase blonanserin AUC by 24 %, compared to a corresponding medium-chain triglyceride solution (Dening et al., 2018).

In the present study, polysorbate 20 presented a dual function in MSH particles with the ability to inhibit P-gp and to facilitate release of digoxin from montmorillonite surfaces. The facilitation of drug release from montmorillonite by polysorbate 20 was also observed by Calabrese and co-workers (Calabrese et al., 2017). 100 % release of the anionic compound, cinnamic acid, was achieved after 6 h from a montmorillonite-polysorbate 20 hybrid, whereas only 80 % was released from pure montmorillonite (Calabrese et al., 2017).

Digoxin-containing montmorillonite retained digoxin and decreased digoxin exposure, while MSH particles increased digoxin exposure. Therefore, changing the ratio between montmorillonite and polysorbate 20 in future formulations may produce enhanced polysorbate 20-mediated P-gp inhibition leading to increased P-gp substrate exposure.

5 Conclusions

The present study is the first to apply a surfactant-containing nanocomposite material to modulate an intestinal efflux transporter, to our knowledge. Characterisation of MSH particles showed that polysorbate 20 affected morphologic appearance of montmorillonite, was intercalated in the interlayer spaces of montmorillonite, and that polysorbate 20 assisted in ordered stacking of montmorillonite layers.

In vivo, MSH particles showed a tendency to increase digoxin exposure *via* P-gp inhibition, both compared to digoxin administered alone and compared with co-administration of corresponding polysorbate 20 doses in simple solutions. Furthermore, digoxin-containing montmorillonite, without polysorbate 20, decreased digoxin exposure. This enhancement in digoxin exposure, when administered as MSH particles, may be caused by mucosa-localised elevated concentrations of both digoxin and polysorbate 20, which led to a more effective inhibition of P-gp. However, more research is required to fully understand the underlying mechanism.

6 Author information

Author contribution

Conception and design of the study: RBN, AK, LD, KW, JS, UGN, RH, and CUN. Acquisition of data: RBN and AK. Analysis and interpretation of data: RBN, AK, LD, KW, JS, UGN, RH, and CUN. Drafting the article: RBN, UGN, RH, and CUN. Critical revising and final approval of the version submitted: RBN, AK, LD, KW, JS, UGN, RH, and CUN.

ORCID

Rasmus Blaaholm Nielsen	0000-0003-1684-215X
Lieve Dillen	0000-0003-0573-9982
Jan Snoeys	0000-0003-3420-424X

Ulla Gro Nielsen 0000-0002-2336-3061

Carsten Uhd Nielsen 0000-0001-5776-6865

Notes: The authors declare no competing financial interests.

7 Acknowledgements

Researchers and technicians at Janssen R&D and The University of Southern Denmark, who helped set up, conduct, and analyse various experiments, including Bjarke Strøm Larsen, Maria Læssøe Pedersen, Nicholai Daugaard Jensen, Dorthe Bomholdt Ravnsbæk, Tae-Hyun Kim, Dries Versweyveld, Sanket Shah, Jasmine Bogaerts, Elene De Cleyn, Kore Van Mechelen, and Luc Sips are hereby acknowledged.

The mobility action related to the project was financially supported by the Erasmus+ Programme, Oticon Fonden, Knud Højgaards Fond, F.W. Frank og Hustru Angelina Franks Mindelegat, and Henry og Mary Skovs Fond.

8 References

Aguzzi, C., Cerezo, P., Viseras, C., Caramella, C., 2007. Use of clays as drug delivery systems: Possibilities and limitations. Appl. Clay Sci. 36, 22-36. https://doi.org/10.1016/j.clay.2006.06.015.

Al-Ali, A.A.A., Nielsen, R.B., Steffansen, B., Holm, R., Nielsen, C.U., 2019. Nonionic surfactants modulate the transport activity of ATP-binding cassette (ABC) transporters and solute carriers (SLC): Relevance to oral drug absorption. Int. J. Pharm. 566, 410-433. https://doi.org/10.1016/j.ijpharm.2019.05.033.

Al-Ali, A.A.A., Quach, J.R.C., Bundgaard, C., Steffansen, B., Holm, R., Nielsen, C.U., 2018a. Polysorbate 20 alters the oral bioavailability of etoposide in wild type and mdr1a deficient Sprague-Dawley rats. Int. J. Pharm. 543, 352-360. https://doi.org/10.1016/j.ijpharm.2018.04.006.

Al-Ali, A.A.A., Steffansen, B., Holm, R., Nielsen, C.U., 2018b. Nonionic surfactants increase digoxin absorption in Caco-2 and MDCKII MDR1 cells: Impact on P-glycoprotein inhibition, barrier function, and repeated cellular exposure. Int. J. Pharm. 551, 270-280. https://doi.org/10.1016/j.ijpharm.2018.09.039.

Al-Saraf, A., Holm, R., Nielsen, C.U., 2016. Tween 20 increases intestinal transport of doxorubicin in vitro but not in vivo. Int. J. Pharm. 498, 66-69. https://doi.org/10.1016/j.ijpharm.2015.12.017.

Aranda, P., Ruiz-Hitzky, E., 1992. Poly(Ethylene Oxide)-Silicate Intercalation Materials. Chem. Mater. 4, 1395-1403. https://doi.org/10.1021/cm00024a048.

Broberg, M.L., Holm, R., Tonsberg, H., Frolund, S., Ewon, K.B., Nielsen, A.L., Brodin, B., Jensen, A., Kall, M.A., Christensen, K.V., Nielsen, C.U., 2012. Function and expression of the proton-coupled amino acid transporter PAT1 along the rat gastrointestinal tract: implications for intestinal absorption of gaboxadol. Br. J. Pharmacol. 167, 654-665. https://doi.org/10.1111/j.1476-5381.2012.02030.x.

490 Calabrese, I., Cavallaro, G., Lazzara, G., Merli, M., Sciascia, L., Liveri, M.L.T., 2016. Preparation
491 and characterization of bio-organoclays using nonionic surfactant. Adsorption 22, 105-116.
492 https://doi.org/10.1007/s10450-015-9697-1.

493 Calabrese, I., Cavallaro, G., Scialabba, C., Licciardi, M., Merli, M., Sciascia, L., Liveri, M.L.T.,
494 2013. Montmorillonite nanodevices for the colon metronidazole delivery. Int. J. Pharm. 457, 224-
495 236. https://doi.org/10.1016/j.ijpharm.2013.09.017.

496 Calabrese, I., Gelardi, G., Merli, M., Liveri, M.L.T., Sciascia, L., 2017. Clay-biosurfactant materials
497 as functional drug delivery systems: Slowing down effect in the in vitro release of cinnamic acid.
498 Appl. Clay Sci. 135, 567-574. https://doi.org/10.1016/j.clay.2016.10.039.

499 Cook, D., Brown, D., Alexander, R., March, R., Morgan, P., Satterthwaite, G., Pangalos, M.N.,
500 2014. Lessons learned from the fate of AstraZeneca's drug pipeline: a five-dimensional framework.
501 Nat. Rev. Drug Discov. 13, 419. https://doi.org/10.1038/nrd4309.

502 Cornaire, G., Woodley, J., Hermann, P., Cloarec, A., Arellano, U., Houin, G., 2004. Impact of
503 excipients on the absorption of P-glycoprotein substrates in vitro and in vivo. Int. J. Pharm. 278,
504 119-131. https://doi.org/10.1016/j.ijpharm.2004.03.001.

505 Dening, T.J., Rao, S., Thomas, N., Prestidge, C.A., 2017. Montmorillonite-lipid hybrid carriers for
506 ionizable and neutral poorly water-soluble drugs: Formulation, characterization and in vitro
507 lipolysis studies. Int. J. Pharm. 526, 95-105. https://doi.org/10.1016/j.ijpharm.2017.04.063.

508 Dening, T.J., Thomas, N., Rao, S., van Looveren, C., Cuyckens, F., Holm, R., Prestidge, C.A.,
509 2018. Montmorillonite and Laponite Clay Materials for the Solidification of Lipid-Based
510 Formulations for the Basic Drug Blonanserin: In Vitro and in Vivo Investigations. Mol. Pharm. 15,
511 4148-4160. https://doi.org/10.1021/acs.molpharmaceut.8b00555.

512 Di, L., Kerns, E.H., 2016. Drug-Like Properties: Concepts, Structure Design and Methods from
513 ADME to Toxicity Optimization, 2nd ed. Academic Press, Boston, USA.

514 Feeney, O.M., Crum, M.F., McEvoy, C.L., Trevaskis, N.L., Williams, H.D., Pouton, C.W.,
515 Charman, W.N., Bergstrom, C.A.S., Porter, C.J.H., 2016. 50 years of oral lipid-based formulations:
516 Provenance, progress and future perspectives. Adv. Drug Deliv. Rev. 101, 167-194.
517 https://doi.org/10.1016/j.addr.2016.04.007.

518 Gurjar, R., Chan, C.Y.S., Curley, P., Sharp, J., Chiong, J., Rannard, S., Siccardi, M., Owen, A.,
519 2018. Inhibitory Effects of Commonly Used Excipients on P-Glycoprotein in Vitro. Mol. Pharm.
520 15, 4835-4842. https://doi.org/10.1021/acs.molpharmaceut.8b00482.

521 Hensen, E.J.M., Smit, B., 2002. Why Clays Swell. J. Phys. Chem. B 106, 12664-12667.
522 https://doi.org/10.1021/jp0264883.

523 Hewitt, D., Alvarez, M., Robinson, K., Ji, J.Y., Wang, Y.J., Kao, Y.H., Zhang, T., 2011. Mixed-
524 mode and reversed-phase liquid chromatography-tandem mass spectrometry methodologies to study
525 composition and base hydrolysis of polysorbate 20 and 80. J. Chromatogr. A 1218, 2138-2145.
526 https://doi.org/10.1016/j.chroma.2010.09.057.

527 Iannuccelli, V., Maretti, E., Montorsi, M., Rustichelli, C., Sacchetti, F., Leo, E., 2015.
528 Gastroretentive montmorillonite-tetracycline nanoclay for the treatment of Helicobacter pylori
529 infection. Int. J. Pharm. 493, 295-304. https://doi.org/10.1016/j.ijpharm.2015.06.049.

530 Kokabi, M., Sirousazar, M., Hassan, Z.M., 2007. PVA-clay nanocomposite hydrogels for wound
531 dressing. Eur. Polym. J. 43, 773-781. https://doi.org/10.1016/j.eurpolymj.2006.11.030.

532 Kola, I., Landis, J., 2004. Can the pharmaceutical industry reduce attrition rates? Nat. Rev. Drug
533 Discov. 3, 711-715. https://doi.org/10.1038/nrd1470.

534 Leslie, E.M., Deeley, R.G., Cole, S.P.C., 2005. Multidrug resistance proteins: role of P-
535 glycoprotein, MRP1, MRP2, and BCRP (ABCG2) in tissue defense. Toxicol. Appl. Pharmacol.
536 204, 216-237. https://doi.org/10.1016/j.taap.2004.10.012.

537 Lin, J.H., Yamazaki, M., 2003. Role of P-glycoprotein in pharmacokinetics - Clinical implications.
538 Clin. Pharmacokinet. 42, 59-98. https://doi.org/10.2165/00003088-200342010-00003.

539 Liu, T.X., Lim, K.P., Tjiu, W.C., Pramoda, K.P., Chen, Z.K., 2003. Preparation and characterization
540 of nylon 11/organoclay nanocomposites. Polymer 44, 3529-3535. https://doi.org/10.1016/s0032-
541 3861(03)00252-0.

542 Lo, Y.I., 2003. Relationships between the hydrophilic-lipophilic balance values of pharmaceutical
543 excipients and their multidrug resistance modulating effect in Caco-2 cells and rat intestines. J.
544 Control. Release 90, 37-48. https://doi.org/10.1016/S0168-3659(03)00163-9.

545 Nair, A.B., Jacob, S., 2016. A simple practice guide for dose conversion between animals and
546 human. J. Basic Clin. Pharm. 7, 27-31. https://doi.org/10.4103/0976-0105.177703.

547 Nielsen, C.U., Abdulhussein, A.A., Colak, D., Holm, R., 2016. Polysorbate 20 increases oral
548 absorption of digoxin in wild-type Sprague Dawley rats, but not in mdr1a(-/-) Sprague Dawley rats.
549 Int. J. Pharm. 513, 78-87. https://doi.org/10.1016/j.ijpharm.2016.09.011.

550 Nohr, M.K., Thale, Z.I., Brodin, B., Hansen, S.H., Holm, R., Nielsen, C.U., 2014. Intestinal
551 absorption of the antiepileptic drug substance vigabatrin is altered by infant formula in vitro and in
552 vivo. Pharmacol. Res. Perspect. 2, e00036. https://doi.org/10.1002/prp2.36.

553 Onnainty, R., Onida, B., Paez, P., Longhi, M., Barresi, A., Granero, G., 2016. Targeted chitosan-
554 based bionanocomposites for controlled oral mucosal delivery of chlorhexidine. Int. J. Pharm. 509,
555 408-418. https://doi.org/10.1016/j.ijpharm.2016.06.011.

556 Ploehn, H.J., Liu, C., 2006. Quantitative Analysis of Montmorillonite Platelet Size by Atomic Force
557 Microscopy. Ind. Eng. Chem. Res. 45, 7025-7034. https://doi.org/10.1021/ie051392r.

558 Rhim, J.W., Park, H.M., Ha, C.S., 2013. Bio-nanocomposites for food packaging applications.
559 Prog. Polym. Sci. 38, 1629-1652. https://doi.org/10.1016/j.progpolymsci.2013.05.008.

560 Ruiz-Hitzky, E., Aranda, P., Darder, M., Rytwo, G., 2010. Hybrid materials based on clays for
561 environmental and biomedical applications. J. Mater. Chem. 20, 9306-9321.
562 https://doi.org/10.1039/c0jm00432d.

563 Sheskey, P.J., Cook, W.G., Cable, C.G., 2017. Handbook of Pharmaceutical Excipients, 8th ed.
564 Pharmaceutical Press, London, UK.

565 Skinner, H.A., 1945. A revision of some bond-energy values and the variation of bond-energy with
566 bond-length. Trans. Faraday Soc. 41, 645-662. https://doi.org/10.1039/tf9454100645.

567 Su, K.S.E., Carstensen, J.T., 1972. Nature of bonding in montmorillonite adsorbates II: Bonding as
568 an ion-dipole interaction. J. Pharm. Sci. 61, 420-424. https://doi.org/10.1002/jps.2600610321.

569 Tan, A., Rao, S., Prestidge, C.A., 2013. Transforming Lipid-Based Oral Drug Delivery Systems
570 into Solid Dosage Forms: An Overview of Solid Carriers, Physicochemical Properties, and
571 Biopharmaceutical Performance. Pharm. Res. 30, 2993-3017. https://doi.org/10.1007/s11095-013-
572 1107-3.

573 Thiebaut, F., Tsuruo, T., Hamada, H., Gottesman, M.M., Pastan, I., Willingham, M.C., 1987.
574 Cellular localization of the multidrug-resistance gene product P-glycoprotein in normal human
575 tissues. Proc. Natl. Acad. Sci. U.S.A. 84, 7735-7738. https://doi.org/10.1073/pnas.84.21.7735.

576 Viani, A., Gaultieri, A.F., Artioli, G., 2002. The nature of disorder in montmorillonite by simulation
577 of X-ray powder patterns. Am. Mineral. 87, 966-975. https://doi.org/10.2138/am-2002-0720.

578 Wang, L., Wang, A.Q., 2007. Adsorption characteristics of Congo Red onto the
579 chitelsan/montmorillonite nanocomposite. J. Hazard. Mater. 147, 979-985.
580 https://doi.org/10.1016/j.jhazmat.2007.01.145.

581 Zhang, H.J., Yao, M., Morrison, R.A., Chong, S.H., 2003. Commonly used surfactant, tween 80,
582 improves absorption of P-glycoprotein substrate, digoxin, in rats. Arch. Pharmacal Res. 26, 768-
583 772. https://doi.org/10.1007/bf02976689.

584

585

9 Figure Legends

Fig. 1: Representative scanning electron microscopy images of A) Untreated montmorillonite, B) digoxin-containing montmorillonite, C) montmorillonite-surfactant hybrid (MSH) particles formulation A, and D) MSH E. ×8700 magnification. Scaling bar = 10 µm.

Fig. 2: Representative runs of thermogravimetric analysis of 2-4 mg aliquots of untreated montmorillonite (MMT), lyophilised montmorillonite (Lyo-MMT), digoxin-containing montmorillonite (DG-MMT), montmorillonite-surfactant hybrid particles (MSH), and polysorbate 20 (PS20). Equilibrated at 30 ^{o}C, heated to 700 ^{o}C at a rate of 10 ^{o}C min^{-1}.

Fig. 3: X-ray diffractograms and *hkl*-indexing of untreated montmorillonite (MMT), lyophilised montmorillonite (Lyo-MMT), digoxin-containing montmorillonite (DG-MMT), and montmorillonite-surfactant hybrid particles (MSH) formulation A (representative of all MSH formulations). Stacked diffractograms, dotted lines represent 0 for each one. Insert: Magnification of 3-8 °. Cu K_{α} radiation source (λ = 1.5406 Å) over the range of 3-50 °2θ with a scan speed of 0.254 ° s^{-1} and a step size of 0.0167 °. Intensity in arbitrary units (a.u.).

Fig. 4: Time-concentration profiles of digoxin after oral administration of 0.2 mg kg^{-1} digoxin to fasted male Sprague Dawley rats (245-300 g) as solutions or suspensions in 40 % v/v ethanol in water. Comparisons of A) digoxin administered alone in solution, with co-administration of 55, 274, or 548 mg kg^{-1} polysorbate 20 (PS20), B) as digoxin-containing montmorillonite (DG-MMT, 548 mg kg^{-1} MMT) or as montmorillonite-surfactant hybrid (MSH) particles containing 55-137 mg kg^{-1} polysorbate 20 (PS20) and 55-137 mg kg^{-1} montmorillonite (MMT) in a 1:1 ratio, and C) as montmorillonite-surfactant hybrid (MSH) particles containing 274-548 mg kg^{-1} MMT and 274-548 mg kg^{-1} PS20 in a 1:1 ratio. D) is an additional representation of selected formulations for direct

comparison. Values are given as mean ± SEM, n=6. All lines are simple connecting lines for overview.

Fig. 5. Illustration of the observed effects of the treatment of montmorillonite with digoxin (blue) or digoxin and polysorbate 20 (red) prior to lyophilisation to form digoxin-containing montmorillonite and montmorillonite-surfactant hybrid (MSH) particles, respectively. Digoxin-containing montmorillonite is exfoliated (no stacking order), and MSH particles elicit increased stacking order and an increase of interlayer distance from 14.9 Å in untreated montmorillonite to 18.0 Å. Overview of the observed effects *in vivo* after oral administration of digoxin-containing montmorillonite and montmorillonite-surfactant hybrid (MSH) particles.

Fig. S1: Scanning electron microscopy images of A) Untreated montmorillonite, B) digoxin-containing montmorillonite, C) montmorillonite-surfactant hybrid (MSH) particles formulation A and D), MSH E. ×430 magnification. Scaling bar = 200 µm.

Fig. S2: Scanning electron microscopy images of lyophilised montmorillonite. A) ×430 and B) ×8700 magnification. Scaling bars = 10 and 200 µm respectively.

Table 1.

Table 2.

Table 3.

Table S1.

10 Supplementary Material

Fig. S1

Fig. S2

Table S1

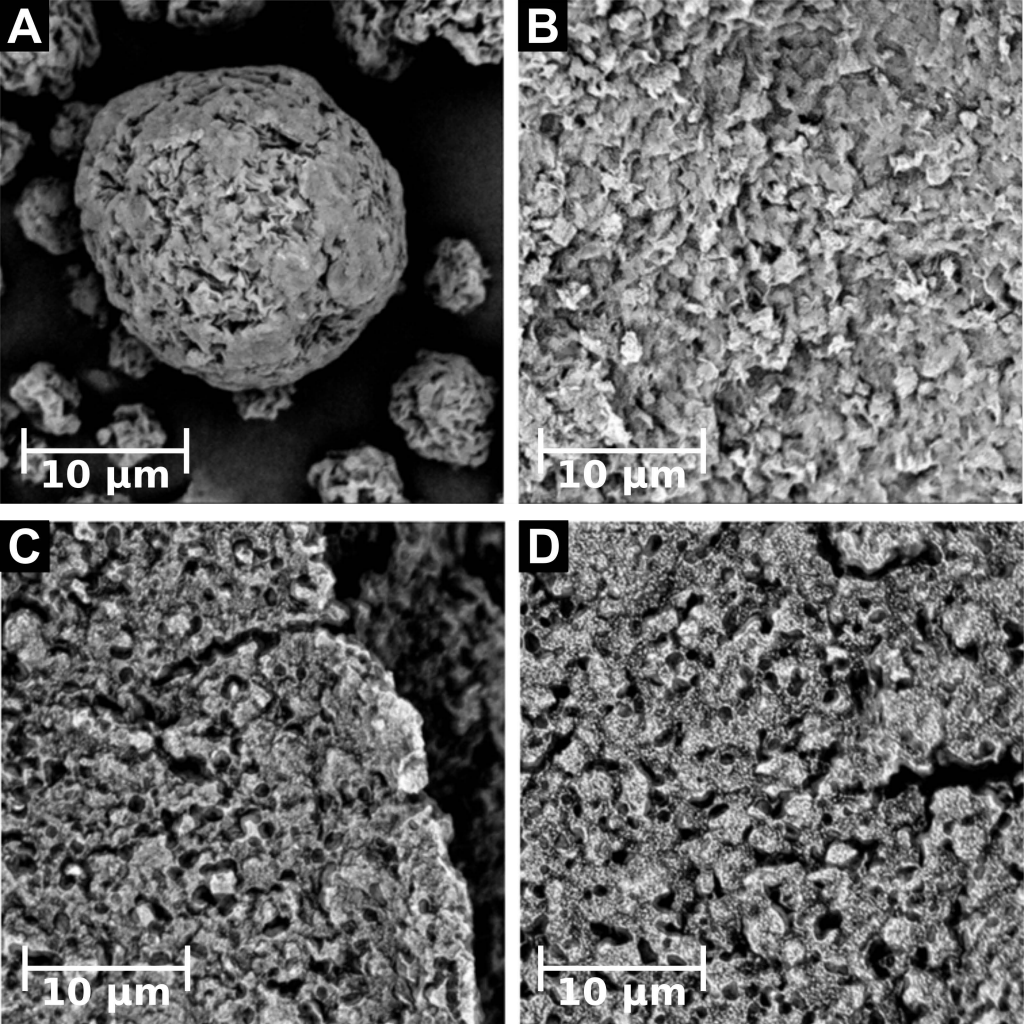
A
10 µm
B
10 µm
C
10 µm
D
10 µm

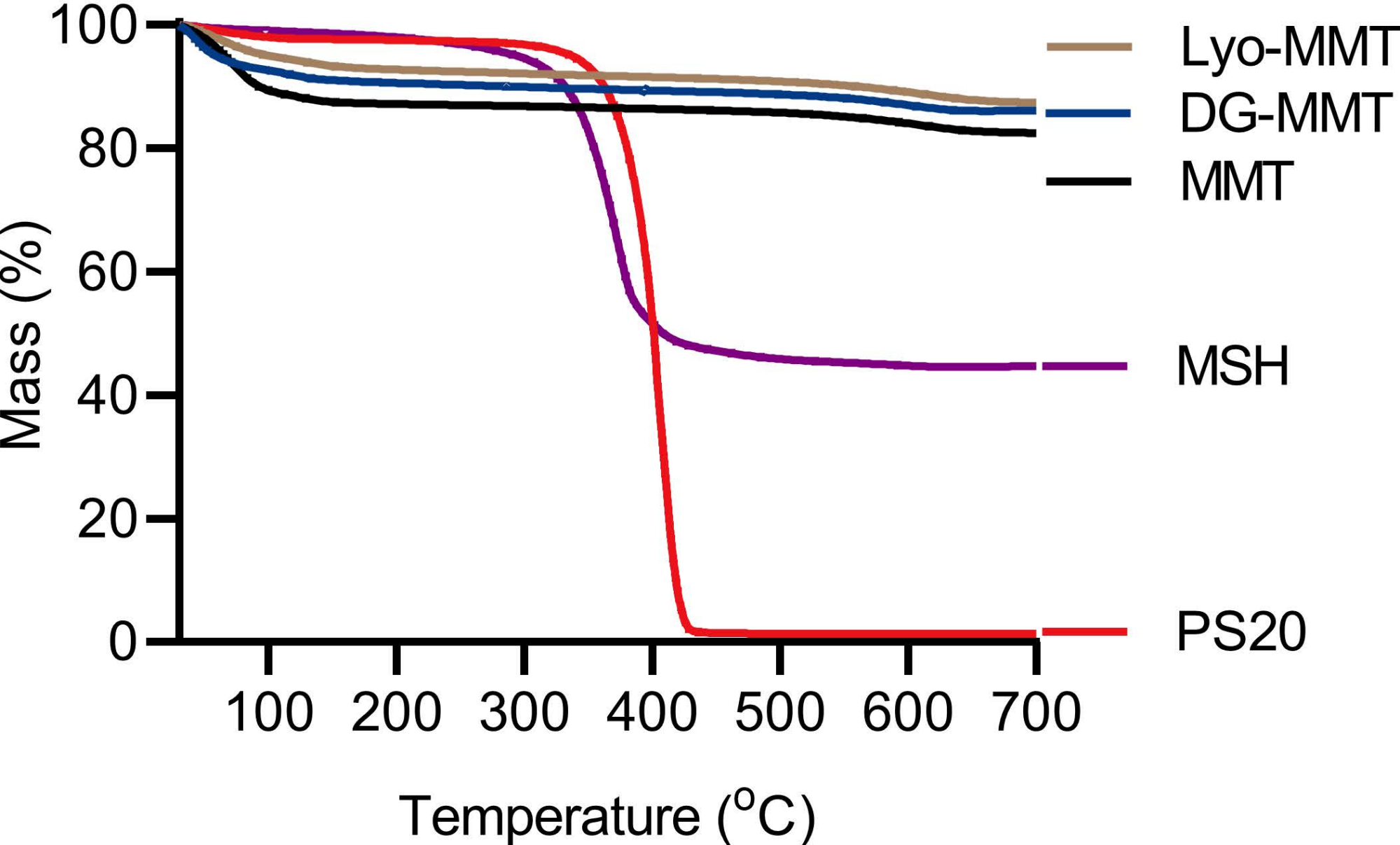
100
80
60
40
20
0
Mass (%)
100
200
300
400
500
600
700
Temperature (°C)
Lyo-MMT
DG-MMT
MMT
MSH
PS20

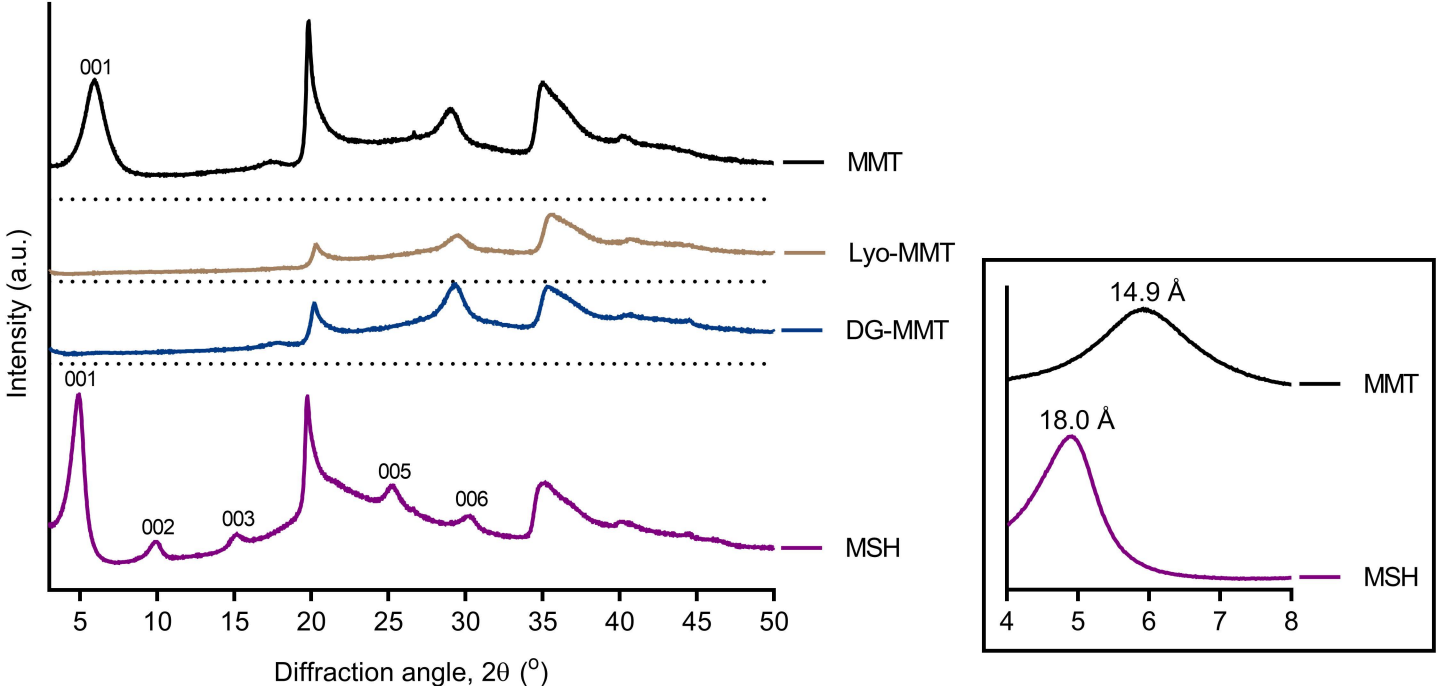
001
MMT
Lyo-MMT
DG-MMT
001
002
003
005
006
MSH
Intensity (a.u.)
5
10
15
20
25
30
35
40
45
50
Diffraction angle, 2θ (°)
14.9 Å
MMT
18.0 Å
MSH
4
5
6
7
8

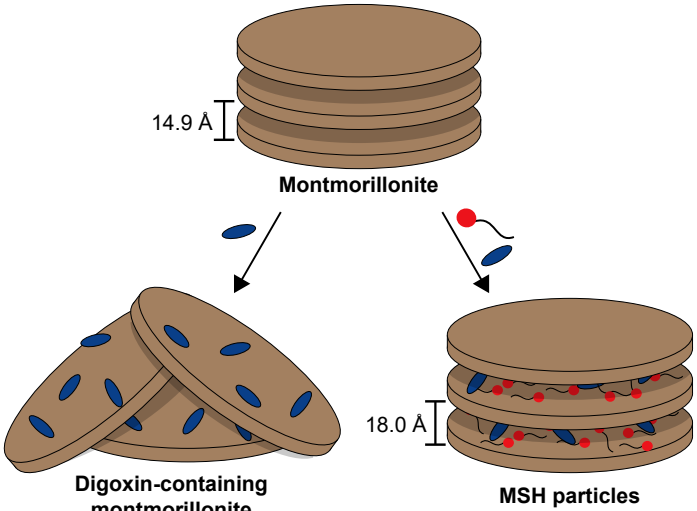

Digoxin adsorption to montmorillonite	Retention of digoxin by montmorillonite	Digoxin release facilitated by polysorbate 20
Intestinal digoxin absorption	Lowered amount available for absorption	Increased absorption
P-gp inhibition	No effect	Enhanced polysorbate 20-mediated P-gp inhibition by local co-release

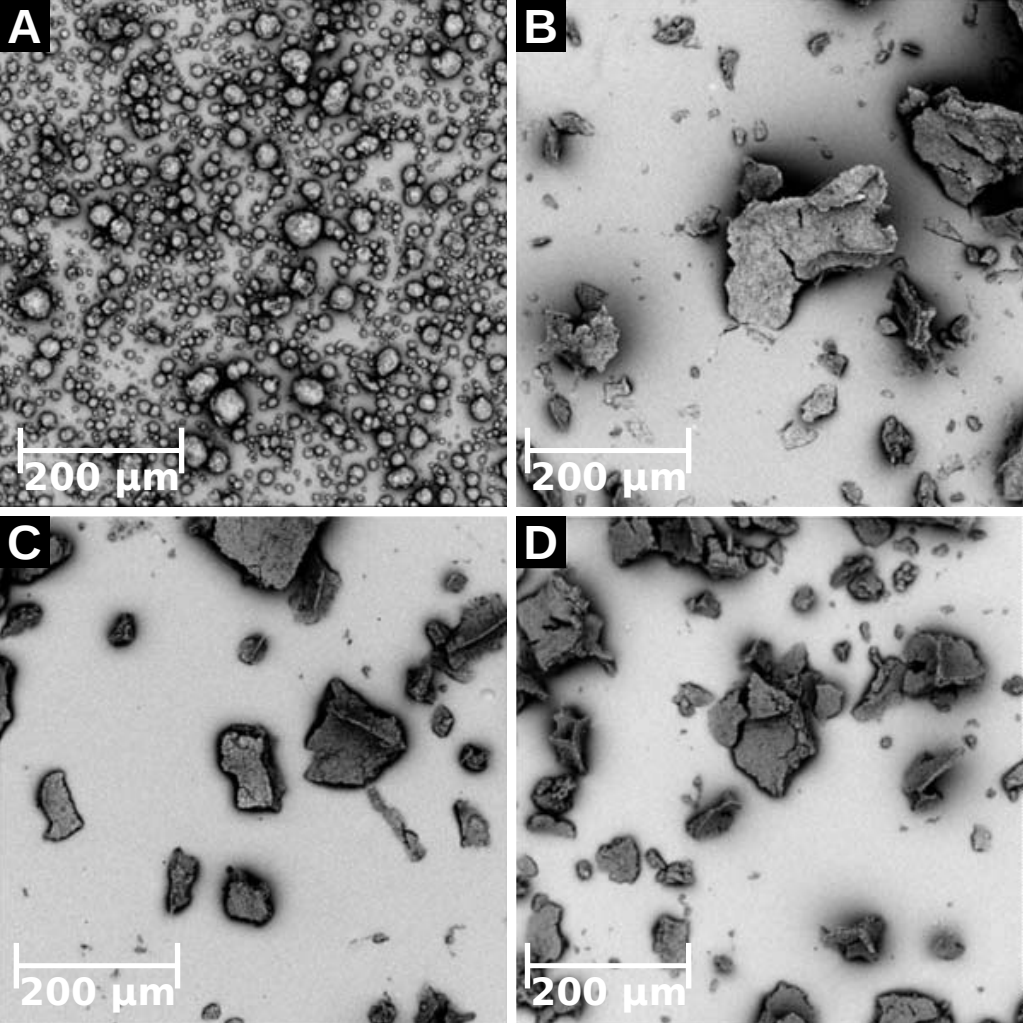
A
200 µm
B
200 µm
C
200 µm
D
200 µm

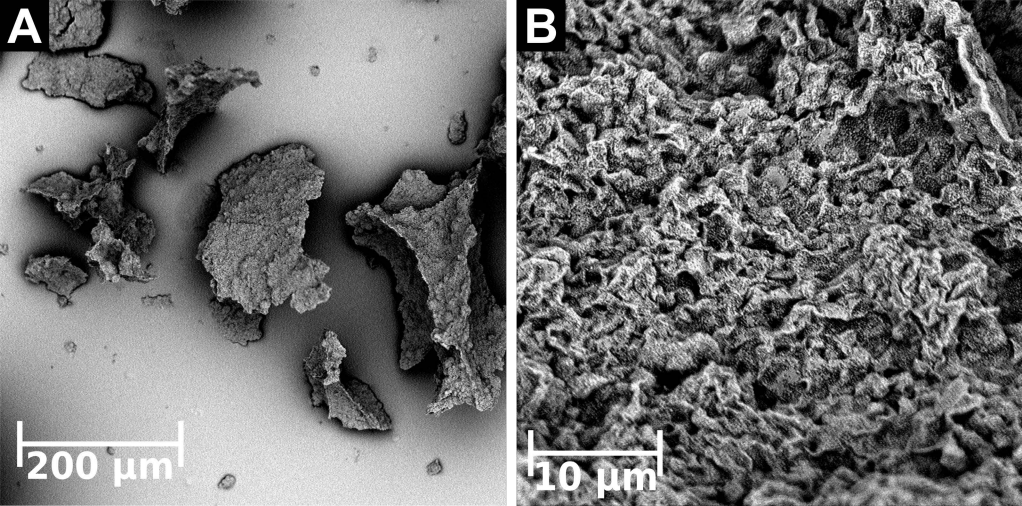
A
200 µm
B
10 µm

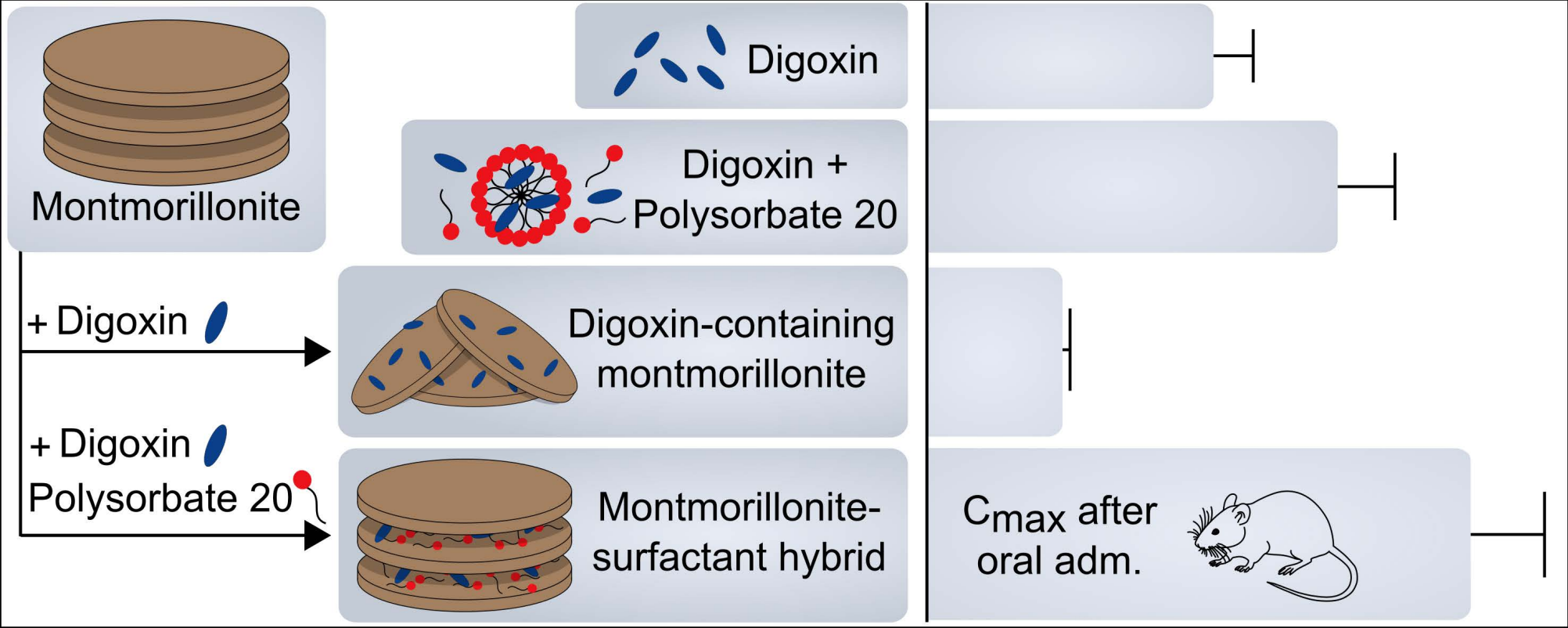
Montmorillonite
+ Digoxin
+ Digoxin
Polysorbate 20
Digoxin
Digoxin +
Polysorbate 20
Digoxin-containing
montmorillonite
Montmorillonite-
surfactant hybrid
Cmax after
oral adm.

Table 1. Overview of prepared formulations

The prepared formulations including the added amounts of montmorillonite, polysorbate 20, and digoxin as well as the calculated final content of these (% w/w).

Formulation	Amount added (mg)			Final content (% w/w)		
	Montmorillonite	Polysorbate 20	Digoxin	Montmorillonite	Polysorbate 20	Digoxin
MSH A	2739	2750	1.00	50	50	0.018
MSH B	2052	2051	1.00	50	50	0.024
MSH C	1368	1372	1.00	50	50	0.036
MSH D	679	689	1.00	50	50	0.073
MSH E	273	275	1.00	50	50	0.182
Lyophilised montmorillonite	2738	-	-	100	-	-
Digoxin-containing montmorillonite	2738	-	1.00	100	-	0.037

MSH, montmorillonite-surfactant hybrid

Table 2. *In vivo* study overview

Overview of administered dose of polysorbate 20, montmorillonite, and digoxin along with the amount of polysorbate 20 in the dosing formulation (% v/v) for each group of male Sprague Dawley rats.

Group number	**1**	**2**	**3**	**4**	**5**	**6**	**7**	**8**	**9**	**10**
Formulation	Solution				Digoxin-containing montmorillonite suspension	MSH particle suspension				
Polysorbate 20 in dosing formulation (% v/v)	-	1	5	10	-	1	2.5	5	7.5	10
Digoxin dose (mg kg^{-1})	0.2	0.2	0.2	0.2	0.2	0.2	0.2	0.2	0.2	0.2
Polysorbate 20 dose (mg kg^{-1})	-	55	274	548	-	55	137	274	411	548
Montmorillonite dose (mg kg^{-1})	-	-	-	-	548	55	137	274	411	548

MSH, montmorillonite-surfactant hybrid

Table 3. Estimated pharmacokinetic parameters.

Formulation	$AUC_{0\text{-}6h}$ ± SEM (µg min mL^{-1})	C_{max} ± SEM (ng mL^{-1})	$C_{15\ min}$ ± SEM (ng mL^{-1})	t_{max} [Q1;Q3] (min)	$t_{½}$ ± SEM (h)
Digoxin	6.05 ± 0.86	29.6 ± 4.9	21.8 ± 1.5	45 [30;60]	2.27 ± 0.15
+ 55 mg kg^{-1} polysorbate 20	6.07 ± 0.46	43.8 ± 4.1	37.9 ± 4.6*	22.5 [15;48.8]	1.76 ± 0.18
+ 274 mg kg^{-1} polysorbate 20	5.75 ± 0.75	41.1 ± 4.0	35.6 ± 3.1*	22.5 [15;33.8]	1.84 ± 0.16
+ 548 mg kg^{-1} polysorbate 20	6.19 ± 0.63	42.6 ± 6.9	34.5 ± 4.2	30 [15;45]	2.42 ± 0.16
Digoxin-containing montmorillonite (548 mg kg^{-1} montmorillonite)	2.78 ± 0.21*	14.1 ± 0.9*	12.6 ± 1.2*	37.5 [15;48.8]	2.78 ± 0.34
MSH (55 mg kg^{-1} montmorillonite & polysorbate 20)	5.14 ± 0.34#	33.0 ± 2.4	27.9 ± 3.5	30 [15;45]	2.46 ± 0.25
MSH (137 mg kg^{-1} montmorillonite & polysorbate 20)	6.81 ± 0.59#	51.2 ± 8.0#	37.3 ± 4.3#	37.5 [30;45]	2.54 ± 0.36
MSH (274 mg kg^{-1} montmorillonite & polysorbate 20)	6.58 ± 0.66#	50.8 ± 7.5#	49.9 ± 7.9*#	15 [15;22.5]	1.99 ± 0.15
MSH (411 mg kg^{-1} montmorillonite & polysorbate 20)	7.71 ± 0.88#	46.7 ± 8.5#	38.6 ± 6.1#	37.5 [15;48.8]	2.30 ± 0.19
MSH (548 mg kg^{-1} montmorillonite & polysorbate 20)	7.94 ± 0.66#	56.4 ± 9.0*#	41.1 ± 4.5*#	30 [30;45]	1.94 ± 0.08

$C_{15\ min}$, the plasma concentration at the first sampling point (15 min); MSH, montmorillonite-surfactant hybrid particles. t_{max} is given as median [25th percentile;75th percentile]. Significantly different from digoxin only marked by * and significantly different from digoxin-containing montmorillonite marked by # ($p < 0.05$).

Table S1. Thermogravimetric mass loss of applied formulations by temperature intervals.

Formulation	Mass lost (%) in temp. interval				
	30 - 100 ºC	**100 - 160 ºC**	**160 - 500 ºC**	**500 - 700 ºC**	**700 ºC**
	Evap. adsorbed water	Evap. interlayer water	Evap. interlayer water + polysorbate 20 decomp.	Montmorillonite dehydroxylation	Residual
Untreated montmorillonite	10.6	2.0	1.6	3.3	82.5
Lyophilised montmorillonite	5.0	1.9	2.3	3.4	87.4
Digoxin-containing montmorillonite	7.4	1.7	2.2	2.6	86.1
Polysorbate 20	2.0	0.3	96.3	0.0	1.4
MSH particles	0.9	0.5	52.7	1.2	44.7

MSH, montmorillonite-surfactant hybrid. The defined intervals were ascribed to evaporation (evap.) of adsorbed water, interlayer water, polysorbate 20 decomposition (decomp.), and montmorillonite dehydroxylation.